JOURNAL OF MOLECULAR SPECTROSCOPY 88, 175–193 (1981)

Laser Spectroscopy of CaBr: $A^2\Pi$–$X^2\Sigma^+$ and $B^2\Sigma^+$–$X^2\Sigma^+$ Systems

P. F. BERNATH[1] AND R. W. FIELD

Spectroscopy Laboratory and Department of Chemistry, Massachusetts Institute of Technology, Cambridge, Massachusetts 02139

AND

B. PINCHEMEL,[2] Y. LEFEBVRE, AND J. SCHAMPS

Laboratoire de Spectroscopie des Molécules Diatomiques, E.R.A. 303, Université des Sciences et Techniques de Lille, Bât. P5, 59655 Villeneuve d'Ascq, France

Laser excitation spectra have been recorded for $Ca^{79}Br$ and $Ca^{81}Br$ in the spectral region 600–630 nm. The use of a 1-m monochromator as a narrow band pass filter (1–2 cm^{-1}) has allowed rotational analysis of the 0–0, 1–1, and 2–2 bands of the $B^2\Sigma^+$–$X^2\Sigma^+$ transition and the 0–0 and 1–1 bands of the $A^2\Pi$–$X^2\Sigma^+$ transition. A few additional lines of the 0–1, 1–2, 1–0, and 2–1 bands of the B–X system were used to obtain band origins for vibrational analysis. The main constants for $Ca^{79}Br$ are (in cm^{-1}):

	$X^2\Sigma^+$	$A^2\Pi$	$B^2\Sigma^+$
T_e	0	15 958.41 (10)	16 383.137 (6)
ω_e	285.732 (9)	288.56 (20)	285.747 (9)
$\omega_e x_e$	0.840 (4)	—	0.954 (4)
B_e	0.094466141 (30)	0.0957343 (20)	0.0965151 (20)
α_e	0.000403551 (40)	0.0004327 (20)	0.0004483 (15)
γ_e (spin–rot.)	0.00301484 (50)	—	0.068767 (79)
p_e	—	−0.066834 (64)	—
A_e	—	59.175 (1)	—

(All uncertainties are 1σ.)

The usual isotope relations between the constants for $Ca^{79}Br$ and $Ca^{81}Br$ are satisfied to within 3σ. The A and B states form a unique perturber pair with l_{eff} = 1.24.

I. INTRODUCTION

The first CaBr spectra were observed by Walters and Barratt in 1928 (*1*). The vibrational assignments appearing in Rosen's tables (*2*) were made by Harrington (*3*) in 1942. The potential curves of the X, A, and B states are very similar, causing the spectra to be extremely congested and overlapped. In addition, there are two isotopes of bromine (^{79}Br, 50.5%; ^{81}Br, 49.5%) of approximately equal abundance.

[1] Present address, Herzberg Institute of Astrophysics, National Research Council of Canada, Ottawa K1A 0R6, Canada.

[2] Visiting scientist at MIT.

0022-2852/81/070175-19$02.00/0

Consequently, no rotational analysis of the $A^2\Pi$–$X^2\Sigma^+$ and $B^2\Sigma^+$–$X^2\Sigma^+$ transitions has been previously performed. The use here of a tunable single-mode, cw dye laser, coupled with selective, narrow bandpass fluorescence detection, has allowed us to assign more than 2000 lines belonging to these two transitions. The A–X and B–X transitions were simultaneously fit using a "direct" approach (*4*). In addition, some X-state microwave transitions, provided by Möller and Törring (*5*), were included in the final fits.

II. EXPERIMENTAL DETAILS

A preliminary study of the A–X and B–X systems was performed in Lille. The CaBr radical was generated from $CaBr_2$ solid, in a King furnace at 1500–2000 K. Fluorescence was excited using a broadband (1 cm^{-1}) CR 590 rhodamine 6G dye laser. Rotational assignments were made using laser-induced fluorescence spectra recorded with a Jobin–Yvon THR 1500 spectrometer and calibrated against thorium lines. This technique has rather limited resolution, ~0.05 cm^{-1}, but the lines recorded and assigned in this way served as a guide for our Doppler-limited laser excitation experiments at MIT.

The excitation spectra were recorded using a Coherent model CR 599-21 dye laser pumped with 4 W from the 5145-Å line of Coherent CR 10 Ar^+ laser. We obtained single-mode powers (<1-MHz bandwidth) of about 30 mW at 6290 Å and 150 mW at 6000 Å using rhodamine 6G dye. Ten percent of the dye laser output power was divided among an I_2 cell, a 300-MHz semiconfocal Fabry–Perot, and a 1.5-GHz spectrum analyzer. The I_2 fluorescence and Fabry–Perot peaks were recorded as calibration at the same time as CaBr excitation spectra. The I_2 lines were assigned using the I_2 atlas of Gerstenkorn and Luc (*6*). The absolute accuracy of the lines is ± 0.003 cm^{-1}, except for blended lines. The line positions and band origins given in this paper have *not* been corrected by subtraction of 0.0056 cm^{-1} as suggested by Gerstenkorn and Luc (*7*).

The CaBr molecule was made in a Broida-type flow system (*8*) by the reaction of Ca metal with CH_3Br. The pressure was typically 0.5 Torr of argon carrier gas (with less than 1% CH_3Br).

The total laser-induced fluorescence was monitored, through a Corning color glass filter (chosen to eliminate scattered laser light), by a Hamamatsu R212 photomultiplier. A typical excitation spectrum of one of the most uncluttered regions of the $B^2\Sigma^+$–$X^2\Sigma^+$ system is shown as the lower trace of Fig. 1. Even with Doppler-limited resolution there is no clear pattern in this badly overlapped spectrum.

Intermodulated fluorescence spectra (*9, 10*) were recorded in order to increase the resolution. This technique is not very useful in this case because, although the lines were better resolved, the pattern of overlapped sequence bands and branches was no clearer. The one exception was in the P_1 branch of the 0–1 band of the $B^2\Sigma^+$–$X^2\Sigma^+$ transition of $Ca^{79}Br$. The low-N and the returning high-N lines near the P_1 head were clearly resolved using intermodulated fluorescence. Hyperfine structure was observed and is the subject of a separate paper (*11*).

The problem in the CaBr A–X and B–X systems is that branches from two isotopes and many sequence bands occur in the same spectral region. However,

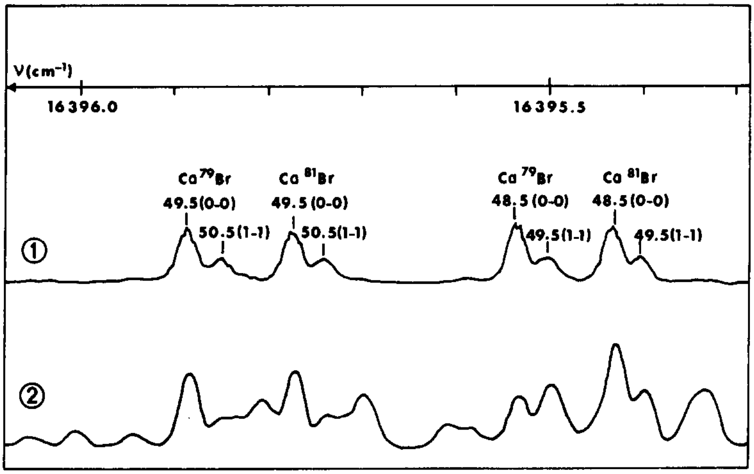

FIG. 1. CaBr $B^2\Sigma^+$–$X^2\Sigma^+$ laser excitation spectrum. This figure illustrates the complexity of the B–X system. One feature, near-overlap of R_1 lines of the 0–0 and 1–1 bands differing by only 1 J unit, would make rotational assignment of a nonlaser spectrum a formidable task. Trace 2 shows the spectrum obtained when total fluorescence is detected. Trace 1 shows the simplification into groups of four lines [0–0 $R_1(J)$ and 1–1 $R_1(J+1)$ for both Br isotopes] that occurs when narrow bandpass fluorescence detection is employed.

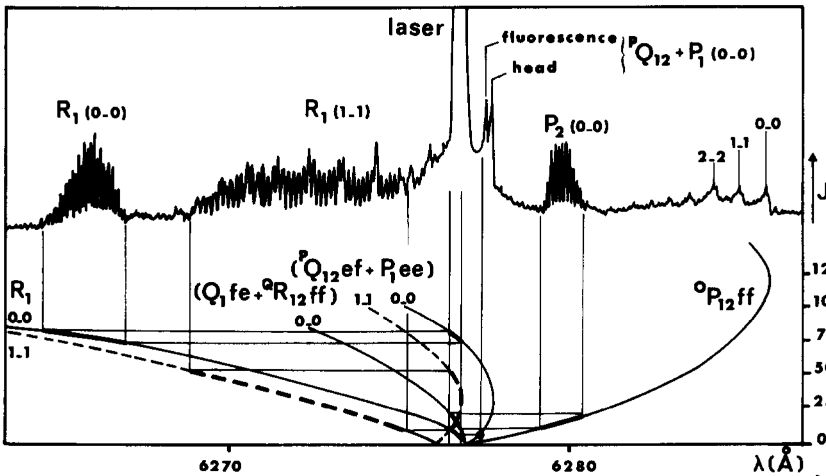

FIG. 2. CaBr $A^2\Pi$–$X^2\Sigma^+$ laser-induced fluorescence spectrum. A Fortrat diagram illustrates the structure of the 0–0 (solid lines) and 1–1 (dotted lines) bands of the A–X system. A 1-cm^{-1} bandwidth laser is tuned to the region of the Q_{12} and P_1 heads of the 1–1 band. The resulting spectrum, shown at the top of the figure, includes a complex pattern of lines, the sources of which are indicated by the heavy portions of the Fortrat parabolas directly under the laser line. Each excitation line is accompanied by a fluorescence line [shifted by approximately $\pm B''(4N+2)$] originating from a common upper level. These lines appear above the heavy portions of the Fortrat parabolas for the conjugate branches. Note that the fluorescence is organized into distinct regions, each associated with a different excitation branch and band combination. This is the basis for success of the selective fluorescence detection laser excitation method.

TABLE I: Measured Line Positions for $Ca^{79}Br$ (in cm^{-1}, * denotes blended line)

TABLE IA. $A^2\Pi_{1/2}$–$X^2\Sigma^+$ System

v'-v"	0 - 0								1 - 1							
J	P_{12ff}	Δν	Q_{1fe}	Δν	R_{12ff}	Δν	R_{1ee}	Δν	P_{12ff}	Δν	Q_{1fe}	Δν	R_{12ff}	Δν	R_{1ee}	Δν
0.5					15 925.091*	4										
			15 925.091*	9	25.152*	-2										
			25.152*	5	25.219*	-4										
			25.220*	6	25.287*	-9										
			25.287*	5	25.369*	-1										
	15 923.229	3	25.357*	4	25.446*	0										
	22.929	6	25.428*	1	25.525*	1										
	-		25.501*	-1	25.611*	6										
	22.326*	3	25.579*	-1	25.691*	3										
	22.027*	0	25.658*	-2	25.775*	2										
10.5	21.736*	2	25.737*	-5	25.866*	5	15 928.708	-4								
11.5	21.446	4	25.819*	-7	-		29.050	-4								
	21.152	0	-		-		29.392	-8	15 923.559 *	7						
	20.865	-1	-		-		29.747	7	23.272 *	8						
	20.581	1	-		26.227*	-6	30.097	1	22.983 *	3						
	-		26.177*	-9	26.325*	-6	30.448	1	-							
	-		26.276*	-6	26.426*	-7	-		22.417 *	0			15 928.811*	8		
	19.741	1	26.374*	-6	26.529*	-7	-		22.138	-1			28.912*	8		
	19.465	1	26.476*	-4	26.634*	-7	31.514	1	21.861	-1	15 928.845*	-4	29.014*	7		
	19.193	3	26.573*	-9	26.742*	-6	31.874	1	21.586	-3	28.945*	-5	29.120*	7	15 934.248	6
20.5	18.922	4	26.681*	-5	26.852*	-7	32.232	-2	21.315	-1	29.052	-1	29.225*	4	34.604	1
21.5	18.654	5	26.786*	-7	26.968*	-2	32.599	1	21.049	1	29.155	-3	29.336*	5	34.961	-4
	-		26.895*	-7	27.091*	7	32.969	4	20.781	1	29.263	-2	29.446*	3	35.330	0
	18.122	3	27.009	-4	27.203*	2	33.336	3	20.517	1	29.372	-2	29.559*	2	35.695	-1
	17.860	3	27.121	-5	27.322*	2			20.253	0	29.483	-3	-		-	
	17.600	3	27.239	-3	27.445*	5			-		29.594	-5	29.790*	-3	-	
	-		27.360	0	27.568*	4			19.736	1	-		29.910*	-4	36.808	0
	17.085	1	27.478	-3	27.693*	4			19.480	1	29.826*	-7	30.032*	-5	37.182	0
	16.833	2	27.602	-1	27.822*	5			19.227	2	29.948*	-5	30.159*	-3	37.564	4
	16.582	2	27.726	-2	27.949*	2			18.973	0	30.070*	-6	30.283*	-6	37.943	4
30.5	-		27.854	-1	28.081*	2			18.725	1	30.195*	-6	30.416*	-3	-	
31.5	-		27.983	-1	28.215*	2			18.479	2	30.322*	-5	30.548*	-3	-	
	15.842	0	28.114	-1	-				-		30.453*	-3	30.694*	9	39.087	0
	15.598	-2	-		-				17.994	4	30.582*	-6	30.819*	-3	39.474	0
	15.357	-3	-		-				17.753	3	30.719	-2	30.958*	-2	39.860	-3
	15.121	-2	.		28.774*	1			17.516	4	30.856	-1	31.100*	-1		
	14.888	-1			28.916*	-3			-		30.994	-1				
	14.656	-1	28.806	0	29.064*	-3			17.045	2						
	14.426	0	28.952	2	29.215*	-2			16.814	2						
	14.199	0	29.100	2	29.365*	-4			16.585	2						
40.5	13.975	2	29.247	0	29.519*	-5										
41.5	13.751	0	29.399	0	29.674*	-7										
	-		29.553	0	29.834*	-6							32.148*	1		
	13.314	2	29.707	-2	29.999*	-3							32.313*	8		
	13.099	3	29.867*	0	30.166*	1			15.472	-1	32.174*	-2	32.475*	9		
	12.885	3	30.027*	-1					15.258	-1	32.331*	-3	32.637*	9		
	12.672*	1	30.188*	-2					15.046	1	32.488*	-5	32.800*	7		
	12.467	5							14.835	0	32.650*	-5	32.967*	6		
	12.259	4							-		32.815*	-4	33.134*	4		
	12.055	4							14.423	3	32.977*	-9	33.305*	4		
50.5	11.853	4			31.198	3			14.223	6	33.147*	-7	-			
51.5	11.650	0			31.380	6			14.019	3	33.321*	-5	33.664*	13		
	11.454	2	31.213*	-2	31.560*	5			13.822	6	-		33.844*	14		
	11.258	1	31.393*	-1	31.745*	6			-		33.664*	-9	34.022*	12		
	11.066	1	31.570*	-4	31.927*	2			-		33.844*	-7	34.204*	11	48.069	1
	10.873*	-1	31.753*	-5	32.117*	3			-		34.022*	-9	34.388*	9	48.504	4
			31.933*	-9	32.308*	4			-		34.204*	-9	34.574*	9	48.937	4
			32.125*	-6	32.502*	5			12.859	3	34.386*	-11	34.764*	10	49.365	-3
			32.312*	-8	32.698*	6	47.542	4	12.673	2	34.574*	-9	34.954*	9	49.801	-4
			32.502*	-10	32.893*	3	47.984	4	12.491	3	34.764*	-8	35.146*	7	50.237*	-7
60.5			32.698*	-9	33.096*	6	48.428	3	12.311	3	34.954*	-9				

fluorescence arising from simultaneous laser excitation of overlapped lines often occurs in different spectral regions, as shown in Fig. 2. Thus, by using a monochromator as a narrow band filter, it is possible to select *only* the fluorescence from a particular branch of a chosen band. The excitation spectrum is then greatly simplified, as shown by the top trace of Fig. 1. In this figure four branches are recorded simultaneously (the R_1 branch of 0–0 and 1–1 bands, for both isotopes) but the pattern is quite clear. By tuning the monochromator from one fluorescence feature to another it is possible to *separately* record all of the branches occurring in a selected region of the spectrum. This technique has been previously applied to CaF (*12*), CaCl (*13*), NO_2 (*14*), and YO (*15*).

TABLE IA—*Continued*

v'-v"	0 - 0								1 - 1							
J	P_{12ff}	Δν	Q_{1fe}	Δν	R_{12ff}	Δν	R_{1ee}	Δν	P_{12ff}	Δν	Q_{1fe}	Δν	R_{12ff}	Δν	R_{1ee}	Δν
61.5			15 932.893 *	-10	15 933.296 *	5	15 948.875	4	15 912.134	-9						
			33.096 *	-7	33.499 *	3	49.314	-6	11.954	0						
			33.296 *	-7	33.707 *	5	49.766	-4	11.784	4						
			33.499 *	-8	-		50.217	-5	11.611	2						
			33.707 *	-6	34.128 *	6			11.446	6						
			-		34.341 *	6			11.277	4						
			34.128 *	-3	34.555 *	4			11.110	1						
			34.341 *	-3	34.772 *	4			10.949	2						
			34.555 *	-3	34.991 *	2										
70.5			34.772 *	-3	35.212 *	2										
71.5			34.991 *	-4	35.438 *	3									15 955.664	2
			35.212 *	-3	35.665 *	3									56.126	1
			35.438 *	-1											56.592	1
			35.665 *	0											57.059	0
	15 907.574 *	6													57.528	-1
	7.434 *	6					55.806	3								
	7.294 *	3					56.284	3								
	7.153 *	-2					56.772 *	11								
	7.020 *	3					57.246	4								
80.5	6.892 *	0					57.726	1								
81.5	6.760	-3					58.209	-2					15 939.959 *	0		
	6.636	-1					58.696	-2					40.202 *	-1		
	6.516	2					59.184	-3			15 939.959 *	0	40.447 *	-2		
	6.393	0					59.679	1			40.202 *	-1	40.698 *	0		
	6.272	-2					60.169	-2			40.447 *	-2	40.951 *	2		
	6.157	-1									40.698 *	1	41.202 *	0		
	6.046	1									40.951 *	4				
	5.934	1									41.202 *	2				
	5.825	1			39.854 *	-6										
90.5	5.721	3			40.122 *	-5										
91.5	5.617	4	39.854 *	3	40.393 *	-4										
	5.515	3	40.122 *	5	40.664 *	-4										
	5.415	2	40.393 *	7	40.937 *	-5										
	5.315*	0	40.664 *	8												
	5.222	0	40.937 *	8												
	-															
	5.039*	0														
	4.954*	1														
	4.870*	2														
100.5	4.791*	5														
101.5	4.709*	4														
	4.628	0														
	4.551	-2														
	4.479	-1														
	4.406	-4														
	4.341	-1														
	4.275	-2														
	4.214	0														
	4.158	4														
110.5	4.098*	2														
111.5	4.038*	-2														
	3.987*	0														
	3.934*	-2														
	3.888*	0														
	3.841*	-1														
	3.797*	-2														
	3.754*	-4														

A 1-m monochromator with 1200-grooves/mm grating was used, in first order, as a filter. The bandpass of the monochromator was set at 1–2 cm^{-1}. A cooled RCA C31034 photomultiplier with photon counting electronics was used to detect the filtered fluorescence.

III. RESULTS

The lines of the 0–0 and 1–1 bands of the $A^2\Pi$–$X^2\Sigma^+$ transition and the 0–0, 1–1, and 2–2 bands of the $B^2\Sigma^+$–$X^2\Sigma^+$ transition of $Ca^{79}Br$ are listed[3] in Table I. The corresponding lines[3] of $Ca^{81}Br$ are in Table II. The assignments were made using standard combination difference relations. Initially, mainly ground-state differ-

[3] Tables I and II were prepared before the microwave data were available so all residuals were obtained from fits that included only optical data. The change in observed–calculated from the combined microwave–optical fits was typically ±0.001 cm^{-1}.

TABLE IB. $A^2\Pi_{3/2}-X^2\Sigma^+$ System

v'-v"	0 - 0								1 - 1							
J	P_{2ff}	Δν	Q_{21fe}	Δν	R_{2ff}	Δν	R_{21ee}	Δν	P_{2ff}	Δν	Q_{21fe}	Δν	R_{2ff}	Δν	R_{21ee}	Δν
5.5	15 987.600*	7			15 989.872*	-13										
	87.331	6	15 989.872*	7	89.989*	-10	15 991.294*	-4								
	87.068	7	89.975*	-2	90.107*	-10	91.602	1							15 994.014	5
	86.805	6	90.090	-1	90.227*	-9	91.909*	2							94.311	-2
	86.545	6	90.206	-2	90.357	-2	92.218	3							94.615	-4
10.5	86.289*	7	90.321	-6	90.475*	-8	92.528*	3							94.926	-1
	86.033	6	90.443*	-6	90.601*	-10	92.837	0							95.240	2
	85.778	3	90.570*	-4	90.732*	-9	93.152	-1							95.558	7
	85.527	2	90.695*	-5	90.866*	-7	-								95.866	-1
			90.823*	-6	91.007*	-2	-								96.183	-3
			90.961*	0	91.146	1	-								96.505	-2
			91.097*	1	91.286	1	-								96.825	-5
			91.234	1	91.427	0	94.770	2	15 986.988	4			15 993.829*	1	97.153	-3
			91.375	3	91.576	3	95.102	3	86.750	2	15 993.776*	2	93.973*	2	97.481	-3
			91.515	2	91.722	2	95.434	2	-		93.915*	1	94.120*	3	97.812	-3
20.5			91.660	2	91.871	1	95.768	0	86.277	-4	94.061*	4	94.269*	4		
			91.806	1	92.023	0	96.109	4	86.049	-3	94.203*	1	94.417*	2		
			91.954	0	92.180	3	96.449	2	85.822	-2	94.352*	3	94.576*	8		
			92.106	0	92.335	1	96.792	1	85.596	-4	94.499*	0	94.725*	2		
			92.262	1	92.496	2	97.140	4	85.375	-3	94.652*	0	94.883*	2		
			92.419	1	92.658	1	97.486	2			94.807*	0	95.044*	3		
			92.577	1	92.821	0	97.837	2			94.964*	0	95.201*	3		
	82.301	2	92.737	-1	92.989	1	98.190	1			95.125*	1	95.371*	3		
	82.089	1	92.901	-2	93.159*	0	98.545	1			95.286*	1	95.539*	3		
	81.880	1	93.069*	0	93.331*	1	98.904	1			95.450*	0	95.710*	4		
30.5	81.674	1	93.239*	1	93.506*	1	99.260	-3			95.617*	0	95.885*	7		
	81.463	-5	93.411*	1	93.670*	-12	99.622	-5			95.788*	2	96.053*	0	16 001.975	0
	81.264	-4	93.583*	-1	93.860*	-2					95.953*	-5	96.232*	2	2.342	5
	81.064	-4	93.757*	-4	94.044*	0					96.128*	-5	96.420*	11	2.704	1
	80.867	-5	93.938*	-1	94.227*	-2					96.303*	-6	96.602*	11	3.069	-2
	80.677	1	94.118*	-3	-						96.488*	0	96.785*	10	3.440	-1
	-		94.305*	-1	-						96.673*	4	96.973*	11	-	
	80.297	-2	-		94.801*	4					96.853*	0	97.162*	11	4.192	4
	80.111	-1	94.683*	2	94.997*	6	16 002.246	4			97.040*	1			4.569	4
	79.926	-3	94.875*	3	-		2.632	6	82.347	2					-	
40.5	79.745	-3	95.068*	2	95.389*	2	3.014	3	82.163						5.328	0
	79.566	-3	95.264*	2	95.589*	0	3.402	1	81.984	1					5.710	-2
	79.388	-5	95.458*	-2	95.792*	-1	-		81.807	1					6.098	-2
	79.216	-4	95.658*	-3	95.999*	-1	4.190	5	81.629	-1					6.487	-1
	79.043	-6	95.859*	-6	96.213*	4	4.587	5	81.457	-1					6.878	-3
	-		96.067*	-4	96.425*	4			81.295	7					7.275	0
	78.714	0	96.282*	2	96.636*	2	5.385	3	81.118	-2						
	78.547	-4	96.493*	2	-		5.787	2	80.953	-2						
	78.388*	-2	-		97.074*	4	6.192	0	80.790	-2						
	78.228*	-3	96.926*	6	97.290*	0	6.599	-1	80.633	1						
50.5	78.073*	-3	97.144*	6	97.512*	-2	7.013	2	80.476	1						
	-		97.359*	1	97.735*	-2			80.321	1						
	77.771*	0	97.588*	6	97.961*	-8			80.168	1						
	77.623*	0	97.806*	-1	98.188*	-11			80.017	1						
	77.476*	-1	98.034*	0	98.425*	-8			79.870	2						
	77.334*	-1	98.260*	-5	98.630*	-4			-							
	77.193*	0	98.495*	-2	98.901*	-5			-							
	-		-		99.144*	-2			-							
	76.922*	2	98.969*	-1	99.386*	-4			-							
	76.790*	3	99.208*	-2	99.633*	-2			79.166	1						
60.5	76.658*	2	99.447*	-5	99.887*	4			79.036	3						
	76.526*	2	99.703*	6	16 000.137*	4			78.904	3						
	76.403*	0	99.948*	4					78.775	2						
	76.279*	0	16 000.189*	-4					78.648	0						
	76.156*	3							78.525	1						
	-								78.403	0						
	-								78.279*	-5						
	75.811*	-1							78.164	-5						
	75.703*	1			1.962*	12			78.051	-4						
	75.597*	4			2.221	1			77.944	0						
70.5	75.492*	4	2.019*	13	2.494	3			77.837*	1						
71.5	15 975.390*	5	16 002.277*	2	16 002.767	2										
	75.290*	6	2.549*	3	3.044	3										
	75.191*	5	2.823*	4	3.317	-2										
	75.097*	6	3.100*	6	3.599	-1										
			3.372*	0	3.884	1	16 018.101	1								
			3.653*	1	-		18.574	-2								
			3.935*	0	4.451	-6	19.055	0								
			-		4.742	-5	19.537	2								
	74.653	3	4.505*	-2	5.038	-2	20.020	2								
80.5	74.570	0	4.795*	-2	5.335	0	-									
	74.491	-1	5.089*	0	5.633	1	20.990	-2								
	74.413	-3	5.384*	2	5.935	3	21.481	-1								
	74.341	-2	5.684*	5	6.237	4	21.974	-1								
	74.269	-3	5.982*	4	6.541	3	22.471	1								
	74.202	-2	6.285*	6			22.968	0								
	74.140	2	6.589*	6												
	74.081	6														

ences were used since, by analogy with CaF and CaCl, the spin–rotation parameter, γ, was expected to be small.

Lines were fit using a weighted (reciprocal, squared uncertainty), nonlinear, least-squares approach ("direct approach") (*4*). The model Hamiltonian includes standard $^2\Pi$ and $^2\Sigma$ matrix elements (*17*). Lambda doubling and spin–rotation

TABLE IC. $B_2\Sigma^+ - X^2\Sigma^+$ System

v'-v"	0 - 0								1 - 1							
J	R_1	Δν	R_2	Δν	P_1	Δν	P_2	Δν	R_1	Δν	R_2	Δν	P_1	Δν	P_2	Δν
1.5																
							16 382.672*	1								
							82.531*	0							16 382.321	0
					16 382.276	0	82.395*	0							82.185	-1
					82.067	0	82.267*	4							-	
	16 384.288*	-9			81.863	0	82.133*	-2							81.931.	4
	84.471*	-11			81.659	-4	82.010*	0							81.812*	9
	84.663*	-8	16 385.616*	-1	81.459	-8										
	84.854*	-10	85.882*	-4	81.273	-2										
10.5	85.054*	-7	86.153*	-6	81.089	2					16 385.923*	-10				
	85.262	0	86.445*	9	80.906	3			16 385.038*	8	86.198*	-10	16 380.697	6		
	85.464	-3	86.729*	11	80.728	5			85.242*	9	86.485*	-2	80.513	2		
	85.674	-2	87.013*	10	80.554	7			85.446*	6	86.767*	-3	80.344	9		
	85.882*	-7	-		80.379	3	81.256*	1	85.654*	4	87.054*	-3	-			
	86.103	-3	87.589*	4	80.215	7	81.166*	2	85.865	0	87.348	0	-			
	86.325	-3	87.885*	3	-		81.079*	3	86.080	-4	87.644	1	-			
	86.553	0	88.185*	2	-		80.996*	4	86.303	-4	87.943	1	79.674	4	80.785	2
	86.783	1	88.493*	5	-		80.916*	3	86.528	-5	88.245	0	79.514	1	80.707	4
	87.017	1	88.799*	2	79.579	1	80.843*	6	86.757	-7	88.549	-3	79.360	-1	80.633	5
20.5	87.253	0	89.114*	4	79.432	1	-		86.992	-6	88.859	-3	79.215	3		
	87.497	2	89.427	0	79.290	2			-		89.174	-3	79.069	1		
	87.735	-5	89.752*	3	79.150	2			87.481	2	89.494	-1	78.918	-9		
	87.988	-2	90.074*	0	79.012	-1			87.733	8	89.815	-2	78.789*	-1		
	88.244	1	90.405*	2	78.883	1			87.974	-2	90.143	-1	78.645*	-12		
	88.497	-4	90.735	-1	78.755	-1			88.229	-1	90.472	-2	78.516*	-14		
	88.761	-2	91.073*	0	78.635	3			88.487	-1	90.807	-1	78.402	-3		
	89.028	0	91.416*	2	78.515	1			88.749	-1	91.146	0	78.284	-1		
	89.299	1	-		78.399	0			89.017	1	91.489	2	78.166	-2		
	89.573	1	92.105*	-3	78.288	-1			89.286	0	91.832	-1	78.054	-2		
30.5	89.852	3	92.456*	-5	78.181	-1			89.560	0	92.180	-2	77.943	-4		
	90.132	1			78.083	3			89.843	6	92.535	1	77.835	-7		
	90.420	3			77.981	0			90.117	-2	92.891	-2	77.739	-3		
	90.704	-2			77.884	-3			90.407	2	-		-			
	91.001				77.794	-3			90.695	1	93.620	0	-			
	91.301	3			77.709	-2			90.989	2	93.990	2	77.453*	-10		
	91.604	4	94.662	1	77.627	-2			91.291	6	94.363	2	-			
	91.908	2	95.041	-1	77.547	-4			91.586	1	94.738	1	77.295	-2		
	92.219	3	95.419	-7	77,477	0			91.892	2	95.119	2	77.218	-3		
	92.532	2	95.809	-6	77.410	3			92.201	2	95.494	-7	77.145	-3		
40.5			96.204	-3	77.340	-2			92.516	4	95.887	-2	77.075	-4		
			96.601	-2					92.829*	0	96.281	0	77.005*	-10		
			96.006	2					93.150*	0	96.676	-7	76.947*	-7		
			97.409	1					93.471*	-3	97.080	4	76.891*	-6		
			97.811	-5					93.799*	-4	97.483*	4	76.843*	-1		
			98.226	-2					94.136	1	97.891*	5	76.790*	-6		
	94.842	4	98.642	-2					94.471	0	98.294	3				
	95.187	3	99.062	-1					94.812	1	98.711	-1				
	95.535	1	99.486	-1					95.157	2	99.129	-1				
	95.891	4	99.915	1					95.503	0	99.554	1				
50.5	96.245	0							95.852	-2	99.979	0				
	96.608	1							96.214	4						
	96.972	0							96.569	0						
	97.343	1					80.660*	-4	96.936	4						
	97.718	3					80.727*	-2	97.301	2						
	98.091	-2					80.807*	9	97.674	4						
	98.473	-1					80.876*	5	98.046	2						
	98.859	0					80.954*	6	98.424	2						
	99.245	-4					81.034*	5	98.806	1						
	99.639	-3					81.119*	6	99.190	0						
60.5	400.035	-5							99.583	2						
61.5									16 399.975	0						
							16 381.706*	2								
							81.820*	4								
							81.937*	5								
							82.054*	1								
							82.189*	1								
70.5							82.305*	1								
71.5							82.437*	1								
			16 410.811*	5												
			11.327*	2												
			11.849	2												
			12.373	0												
			12.898	-6												
80.5																
81.5																
									411.033	-4						
									11.530	3						
									12.024	3						
									12.521	2						
90.5									13.023	3						

TABLE IC—*Continued*

	2 - 2							
	R_1	Δν	R_2	Δν	P_1	Δν	R_2	Δν
11.5								
			16 386.305	-5				
			86.591	-4				
			86.880	-3				
	16 385.832*	-1						
	86.056*	-2	87.774	1				
	86.280*	-3	88.078	2				
20.5			88.385	0				
			88.697	1				
			89.015	4				
	87.481	2						
	87.734	4						
	87.988	4						
	88.244	2			16 377.833*	6		
					77.708	0		
					77.594	1		
30.5					77.481	-1		
					77.377	1		
	89.591	-1			77.274	1		
	89.870	-3			77.172	-1		
	90.158	0			77.078	0		
					76.989	2		
	90.737	-3			76.897	-2		
	91.037	1			76.813	-3		
	91.338	1			76.737	1		
	91.643	2			76.658	-2		
40.5	91.951	2			76.581*	-7		
	92.264	3			76.520*	0		
	92.579	2			76.453*	-3		
	92.897	1			76.393*	-3		
	93.213	-6			76.340*	1		
	93.540	-6			76.290*	3		
	93.872	-5			76.244*	5		
	94.213	1			76.201*	7		
	94.552	2			76.161*	8		
	94.892	-1						
50.5	95.241	3						
	95.591	2						
	95.940	-2						
	96.299	-1						
	96.662	1						
	97.027	1						
	97.398	4						
	97.765	-2						
	98.140	-3						
	98.521	-2						
60.5	98.907	0						
	99.295	1						
	99.686	1						
	16 400.080	0						

effects were accounted for in each state with the usual second-order perturbation theory expressions (*4*). The uncertainties of well resolved and blended lines are taken at 0.005 and 0.01 cm^{-1}, respectively. For each isotope, the $v = 0$ levels of B, A, and X states were fit simultaneously. Similar fits were made for $v = 1$. The 2–2 band of the B–X system of $Ca^{79}Br$ was fit alone with γ_D' fixed at the value obtained for the $v = 0$ level. For the B–X 2–2 band of $Ca^{81}Br$, D'' and γ'' were fixed at values linearly extrapolated from $v'' = 0$ and 1 levels.

After our optical analysis was complete, Möller and Törring provided 40 microwave transitions for $X\,^2\Sigma^+$ $v'' = 0$, 1, and 2 of both isotopes. These data include high-N (~50) and low-N (~50) transitions of about 40-kHz (1.3×10^{-6} cm^{-1}) accuracy. These transitions were included in our final fits. The microwave transitions greatly improved the ground-state constants and reduced the correlation between ground- and excited-state constants.

TABLE II: Measured Line Positions for $Ca^{81}Br$ (in cm^{-1}, * denotes blended line)

TABLE IIA. $A^2\Pi_{1/2}$–$X^2\Sigma^+$ System

v'-v"	0 - 0								1 - 1							
J	P_{12ff}	Δν	Q_{1fe}	Δν	R_{12ff}	Δν	R_{1ee}	Δν	P_{12ff}	Δν	Q_{1fe}	Δν	R_{12ff}	Δν	R_{1ee}	Δν
0.5					15 925.091*	10										
			15 925.091*	14	25.152*	3										
			25.152*	11	25.220*	2										
			25.220*	13	25.287*	-2										
			25.287*	11	25.367*	6										
	15 923.229*	-7	25.357*	11	25.446*	7										
	22.929*	-7	25.428*	9	25.525*	9										
			25.501*	8	25.611*	15										
	22.335*	-6	25.579*	8	25.691*	13										
	22.037	-10	25.658*	8	25.775*	12										
10.5	21.758	2	25.737*	5	25.866*	16										
11.5	21.464	-3	25.819*	3			15 929.010	-7								
	21.177	-3					29.351	-7	15 923.559*	-7						
	20.893	-2							23.272*	-9						
	20.611	-1			26.227*	8	30.047	-3	22.994*	-5						
			26.177*	4	26.325*	8	30.396	-1								
			26.276*	8	26.426*	9			22.439	-2			15 928.774	-2		
	19.778	0	26.374*	9	26.529*	10			22.165	0			28.874	-2		
	19.504	0	26.476*	12	26.634*	11	31.451	-4	21.891	0	15 928.811*	-9	28.979	0		
	19.234	1	26.573*	8	26.727	-3	31.810	-2	21.619	-1	28.912*	-8	29.084	0	15 934.175	4
20.5	18.967	3	26.665	-3	26.837	-2	32.168	-3	21.350	0	29.014*	-8	29.193	2	34.528	0
21.5	18.699	2	26.772	-2	26.949	-1	32.529	-3	21.085	2	29.120*	-6	29.299	-1	34.888	1
			26.878	-4	27.061	-2			20.820	1	29.225*	-7	29.411	-1	35.250	1
	18.172	1	26.983*	-10	27.173	-6	33.263	2	20.557	1	29.336*	-5	29.524	-1	35.614	1
	17.913	2	27.091*	-14	27.291	-6	33.630	2	20.296	1	29.448*	-5				
	17.656	3	27.203*	-17	27.413	-4					29.559*	-5	29.754	-5		
					27.536	-3			19.784	2			29.876	-3	36.717	2
	17.147	1	27.445*	-11	27.661	-2			19.530	2	29.790*	-6	29.996	-6	37.087	-1
	16.894	1	27.568*	-10	27.786	-3			19.279	2	29.910*	-6	30.121	-5	37.462	1
	16.645	0	27.693*	-8	28.916	-3			19.030	3	30.032*	-5	30.249	-4	37.841	4
30.5			27.822*	-5	28.047	-2			18.782	2	30.159*	-2	30.382	0		
31.5			27.949*	-6	28.182	-1			18.537	2	30.283*	-3	30.512	-1		
	15.912	0	28.081*	-5							30.417*	2	30.646	0	38.978	1
	15.672	-1							18.058	5	30.550*	5	30.784	2	39.358	-3
	15.432	-3							17.818	3	30.684*	6	30.920	1	39.745	-3
	15.201	0			28.738	-1			17.583	4	30.819*	7	31.061	2		
	14.966	-2			28.884	0					30.958*	9				
	14.735	-2	28.774*	3	29.030	0			17.115	0						
	14.512	3	28.916*	2	29.177	-2			16.887	1						
	14.284	1	29.064*	4	29.330	0			16.658	-1						
40.5	14.059	0	29.215*	6	29.481	-2			16.436	1						
41.5	13.838	0	29.365*	6	29.637	-2										
			29.518*	6	29.794	-3							32.104*	6		
	13.406	2	29.674*	7	29.956	-1							32.256*	1		
	13.191	1	29.824*	1	30.117	-2					32.120*	-1	32.418*	3		
	12.980	2	29.982*	-1					15.348	2	32.280*	2	32.580*	3		
	12.770	2	30.142*	-2					15.136	0	32.440*	4	32.745*	4		
									14.925	-1	32.596*	-2	32.907*	0		
	12.361	5							14.720	-1	32.755*	-6	33.082*	8		
	12.158	4							14.519	2	32.923*	-3	33.253*	8		
50.5	11.958	5			31.143*	3			14.316	1	33.082*	-10				
51.5	11.757	2			31.321*	2			14.118	2	33.253*	-10				
	11.564	4	31.158*	-2	31.492*	-6			13.919	1			33.775*	6		
	11.369	3	31.336*	-2	31.679*	-2			13.726	2			33.954*	5		
	11.177	1	31.518*	1	31.867*	1					33.775*	-9	34.134*	4	47.887	-2
	10.990	3	31.689*	-10	32.054*	2					33.954*	-8	34.317*	3	48.316	0
	10.804	3	31.877*	-6	32.250*	8					34.134*	-9	34.502*	3	48.748	1
			32.065*	-4	32.439*	6					34.317*	-9	34.692*	5	49.181	3
			32.250*	-7	32.633*	6			12.783	-1	34.502*	-9	34.880*	3	49.605	-6
			32.439*	-9	32.827*	5	47.793	3	12.601	-2	34.692*	-6	35.072*	3	50.038*	-9
60.5			32.633*	-8	33.024*	3	48.231	4	12.424	0	34.881*	-6				

The spectroscopic constants obtained from these fits are given in Table III. One extra digit is retained so that the constants will reproduce the original data.

In order to perform a vibrational analysis of the $B^2\Sigma^+$–$X^2\Sigma^+$ system, we recorded a few lines from bands of $\Delta v = \pm 1$ sequences. These lines are listed in Table IV. The assignments were made by calculating spectra using the constants of Table III and estimated band origins obtained from the bandheads given in Table V. These lines were then used to determine the band origins in Table VI.

Table VII contains the equilibrium constants of X, A, and B states for both isotopes. For the A state we used the Pekeris relationship (*18*) to obtain $\omega_e x_e$. All Franck–Condon factors greater than 0.001 for vibrational levels less than $v = 5$ for the A–X and B–X transitions appear in Table VIII. They were calculated using standard RKR (*19*) and FCF (*20*) programs from $Ca^{79}Br$ equilibrium constants.

TABLE IIA—*Continued*

v'-v''	0 – 0								1 – 1							
J	P_{12ff}	Δν	Q_{1fe}	Δν	R_{12ff}	Δν	R_{1ee}	Δν	P_{12ff}	Δν	Q_{1fe}	Δν	R_{12ff}	Δν	R_{1ee}	Δν
61.5			32.827*	-9	33.226*	5	48.679	5	12.248	0	35.072	-6				
			33.024*	-10	33.428*	4	49.123	4	12.078	4						
			33.226*	-7	33.632*	3	49.570	3	11.907	4						
			33.428*	-7	33.840*	4	50.010	-4	11.737	5						
			33.632*	-7	34.050*	5	50.461	-5	11.565	-1						
			33.840*	-5	34.265*	8			11.397	-3						
			34.050*	-4	34.478*	8			11.237	-1						
			34.265*	0	34.694*	8			11.072	-6						
			34.478*	0					10.915	-5						
70.5			34.694*	1	35.127*	2										
71.5					35.349*	1										
			35.127*	-3	35.575*	3									55.884*	3
			35.349*	-3	35.803*	3									56.345*	2
			35.575*	-1											56.804*	-4
			35.803*	1											57.274*	1
							56.028	1								
	7.293*	-7					56.508	6								
	7.165*	-4					56.983	3								
80.5	7.034*	-5					57.464	4								
81.5	6.909*	-3					57.938	-4					39.845*	-6		
	6.784	-4					58.421	-4					40.088*	-6		
	6.663	-3					58.907	-4			39.946*	3	40.332*	-7		
	6.545	0					59.396	-2			40.088*	4	40.578*	-7		
	6.429	0					59.886	-5			40.332*	4	40.832*	-3		
	6.311	-2					60.375	-2			40.578*	4	41.082*	-4		
	6.199	-2									40.832*	9	41.335*	-5		
	6.089	-2									41.082*	9				
	5.984	1									41.335*	9				
90.5	5.882	4			40.000*	-4										
91.5	5.775	1			40.264*	-7										
	5.677	3	40.000*	6	40.535*	-6										
	5.579	3	40.264*	4	40.807*	-5										
	5.484	4	40.535*	6	41.081*	-6										
	5.390	3	40.807*	7												
	5.305*	9	41.081*	7												
	5.213*	5														
	5.039*	2														
100.5	4.954*	-2														
101.5	4.870*	-7														
	4.791*	-10														
	4.720*	-6														
	4.650*	-5														
	4.581*	-5														
	4.513*	-6														
	4.452*	-3														
110.5																

IV. DISCUSSION

In the calcium halides, the $X^2\Sigma^+$ state is derived from the slightly antibonding $4s\sigma$ molecular orbital centered on Ca^+. The $A^2\Pi$ and $B^2\Sigma^+$ states seem to form a $4p$ complex, split by the ligand field of the halide. Thus the A–X and B–X transitions are the molecular analogs of the atomic resonance lines of a one valence electron atom. By analogy with CaF (*12, 21*) and CaCl (*13, 22*), the A and B states are expected to form a unique perturber pair (*4*) with l slightly greater than 1. Using $l = 1$, the pure precession relationship (*23*) predicts $\gamma_0 \approx p_0 = -0.0529\ \text{cm}^{-1}$. As can be seen from Table III, $\gamma_0 \approx p_0$ but both are 27% larger than this value. This implies an $l_{\text{eff}} = 1.24$ for the expression

$$\frac{2ABl_{\text{eff}}(l_{\text{eff}} + 1)}{\Delta\nu_{\Sigma-\Pi_{1/2}}}.$$

The simplest explanation of this is that the p complex contains some $3d$ character which increases the l value toward 2. There is a trend in the calcium halides for an increase in l_{eff} from 1.04 in CaF (*12*), 1.12 in CaCl (*13*) to 1.34 in CaI (*24*).

The Franck–Condon factors for the A–X and B–X systems (Table VIII) are

TABLE IIB. $A^2\Pi_{3/2}$–$X^2\Sigma^+$ System

v'-v"	0 - 0								1 - 1							
J	P_{2ff}	Δν	Q_{21fe}	Δν	R_{2ff}	Δν	R_{21ee}	Δν	P_{2ff}	Δν	Q_{21fe}	Δν	R_{2ff}	Δν	R_{21ee}	Δν
5.5	15 987.600*	-2			15 989.872*	3										
	87.331*	-5	15 989.872*	16	89.989*	0	15 991.280*	3								
	87.068*	-5	89.975*	9	90.107*	2	91.580	3							15 993.974	0
	86.805*	-9	90.090*	10	90.227*	3	91.880	0							94.273	-2
	86.545*	-11	90.206*	11	90.357*	11	92.184	-1							94.575	-3
10.5	86.289*	-12	90.321*	7	90.475*	6	92.493	0							94.883	0
11.5	86.046*	-3	90.443*	8	90.601*	6	92.800	-3							95.194	1
	85.790*	-8	90.570*	12	90.732*	8	93.115	-1							95.506	0
	85.547*	-3	90.695*	12	90.866*	11									95.823	7
			90.823*	11	90.994*	5									96.131	-1
			90.950*	8	91.130*	4									96.451	0
			91.080*	4	91.268*	4									96.770	-1
			91.214*	3	91.408	3			15 987.008	2			15 993.792*	-3	97.093	-1
			91.353	4	91.553	5	95.048	2	86.769	-2			93.936*	-1	97.419	-1
			91.495	5	91.698	3	95.377	0			15 993.882	3	94.081	-1	97.747	-1
20.5			91.636	3	91.845	2	95.707	-3	86.305	-4	94.023	3	94.230	1		
21.5			91.780	1	91.994	0	96.046	1	86.071	-10	94.167	3	94.379	1		
			91.929	2	92.149	1	96.384	1	85.856	-1	94.313	2	94.531	1		
			92.079	1	92.303	-1	96.727	4	85.632	-2	94.461	2	94.685	1		
			92.232	1	92.462	-1	97.069	3	85.413	-1	94.612	1	94.841	5		
			92.387	1	92.621	-2	97.412	0			94.765	1	95.002	2		
			92.542	-2	92.787	0	97.760	0			94.921	1	95.163	2		
	82.352	1	92.702	-2	92.951	-1	98.111	1					95.326	1		
	82.143	2	92.866	-1	93.120	-1	98.462	-1			95.240	1	95.492	1		
	81.936	3	93.031	-1	93.290	-2	98.819	1			95.403	1	95.663	3		
30.5	81.731	2	93.199	-1	93.465	-1	99.172	-5			95.569	2	95.829	-2		
31.5			93.370	-1	93.638	-2	99.531	-6			95.738	2	95.998	-6		
	81.323	-4	93.540	-3	93.816	-3					95.897	*-9	96.176	-4	16 002.237	3
	81.126	-4	93.715	-3	93.996	-3					96.071	*-8	96.354	-3	2.602	6
	80.931	-4	93.893	-3	94.180	-2					96.246	*-8	96.540	2	2.960	-1
	80.737	-6	94.073	-3	94.372	4					96.433	* 1	96.725	4	3.324	-4
			94.255	-3	94.560	4					96.613	* 2	96.908	1		
	80.362	-4	94.445*	2	94.748	2					96.785	*-8	97.094	0	4.073	3
	80.180	-2	94.628*	-2	94.944	5					96.973	*-5			4.448	5
	79.998	-1	94.818*	-2	95.137	3	16 002.514	4	82.407	0						
40.5	79.817	-3	94.999*	-13	95.335	3	2.895	2	82.227	1					5.198	-1
41.5	79.641	-2	95.197*	-10	95.533	1	3.279	0	82.048	0					5.582	1
	79.464	-4	95.397*	-7	95.734	0			81.871	-1					5.964	-1
	79.292	-4	95.597*	-6			4.060	4	81.697	-2					6.350	-1
	79.122	-5			96.146	0	4.452	2							6.738	-1
	78.955	-5	96.005*	-5	96.356	0			81.358	-2					7.130	-1
	78.794	0	96.213*	-4	96.568	0	5.243	0	81.190	-3						
	78.633	0	96.425*	-1			5.642	-1	81.028	-2						
	78.471	-2	96.636*	-1	97.005	5	6.046	0	80.867	-1						
	78.315	-1			97.217	-2	6.450	-2	80.708	-3						
50.5	78.161	-1	97.074*	+6	97.438	-3	6.856	-3	80.554	0						
51.5	78.005*	-4	97.286*	0	97.664	-1	7.269	0	80.401	1						
	77.858	-2	97.509*	1	97.888	-4			80.247	-1						
	77.712	-1	97.736*	5	98.115*	-6			80.100	0						
	77.567	-1	97.964*	6	98.344*	-9			79.953	-1						
	77.425	-1	98.188*	2	98.580*	-6										
	77.285	-2	98.425*	9	98.818*	-4										
	77.149	-1			99.057*	-4										
			98.887*	2	99.298*	-3										
	76.885*	2	99.124*	1	99.549	4										
60.5	76.760*	6	99.365*	2	99.795	5			79.125	0						
61.5	76.632*	5	99.611*	5	16 000.046	7			78.994	-2						
	76.512*	10	99.856*	5					78.867	-2						
	76.387*	6	16 000.101*	2					78.745	0						
	76.266*	5							78.624	1						
	76.156*	12							78.506	3						
									78.387	1						
									78.279*	8						
	75.811*	3							78.164*	5						
	75.703*	2			2.109	1			78.051*	2						
70.5	75.597*	1	1.909*	12	2.378	0			77.944*	3						
71.5	75.492*	-2	2.165*	1	2.652	3			77.837*	0						
	75.390*	-4	2.436*	4	2.925	1										
	75.290*	-7	2.705*	2	3.205	5										
	75.198*	-5	2.980*	4	3.475	-3										
	75.105*	-6	3.255*	3	3.758	-2	17.854	0								
	75.019*	-3	3.528*	-2	4.042	-1	18.326	-1								
			3.812*	1	4.330	1	18.799	-2								
					4.610	-7										
			4.374*	-5	4.904	-4	19.759	3								
80.5			4.661*	-5			20.240	3								
81.5	74.610*	0	4.952*	-4	5.494	-1	20.722	1								
	74.535*	0	5.248*	1	5.793	1	21.205	-2								
	74.464*	0	5.542*	0	6.092	0	21.697	1								
	74.400*	6	5.839*	1	6.396	2	22.186	-2								
	74.332*	6	6.139*	2	6.700	2	22.682	1								
	74.269*	8	6.441*	2			23.178	1								
	74.202*	3														
	74.140*	1														
	74.081*	0														
90.5																
91.5																

TABLE IIC. $B^2\Sigma^+$–$X^2\Sigma^+$ System

v'-v"	0 - 0								1 - 1							
J	R_1	Δν	R_2	Δν	P_1	Δν	P_2	Δν	R_1	Δν	R_2	Δν	P_1	Δν	P_2	Δν
0.5																
							16 382.672	5								
							82.531	3							16 382.321	2
					16 382.276	1	82.395	2							82.185	5
					82.067	-2	82.267	5								
	16 384.288	7			81.863	-3	82.133	-2							81.931	4
	84.471	7			81.659	-9	82.010	-1							81.812	8
	84.663	11	16 385.593	4	81.459	-14	81.906	13								
	84.853	9	85.855	-1	81.273	-10										
10.5	85.052	13	86.124	-2	81.089	-8										
11.5	85.247	9	86.401	0	80.912	-2							16 380.697	-7		
	85.457	15	86.681	0	80.728	-8					16 386.445	-5	80.520	-5		
	85.654	5	86.965	2	80.554	-7			16 385.419	4	86.729	-2	80.350	0		
	85.864	4			80.383	-8	81.256	-6	85.630	6	87.013	-3	80.180	1		
	86.082	6	87.542	1	80.215	-6	81.166	-5	85.841	4			80.006	-7		
	86.302	5	87.838	3			81.079	-6	86.054	0	87.589	-8				
	86.524	5	88.136	2			80.996	-6	86.278	3	87.885	-8	79.695	4	80.785	-7
	86.751	4	88.437	0			80.916	-7	86.499	-1	88.185	-9	79.541	5	80.709	-4
	86.985	6	88.744	1	79.592	-9	80.843	-5	86.725	-4	88.492	-5	79.388	4	80.633	-4
20.5	87.225	11	89.053	-1	79.454	-1			86.960	-2	88.798	-7	79.237	-1	80.564	-1
21.5	87.442	12	89.369	1	79.312	-1	80.709	-1			89.112	-5	79.093	-1		
	87.690	-7	89.687	1	79.175	-1			87.442	3	89.427	-6	78.951	-4		
	87.939	-6	90.010	1	79.040	-2			87.690	8	89.750	-3	78.820	1		
	88.193	-4	90.336	1	78.915	3					90.074	-2	78.680	-8		
	88.449	-4	90.666	0	78.739	2					90.404	0	78.546	-15		
	88.711	-1	91.001	1	78.666	1					90.735	-1	78.434	-3		
	88.976	0	91.341	2	78.554	7					91.073	2	78.318	1		
	89.245	2	91.684	3	78.437	3					91.416	6	78.197	-5		
	89.514	-1	92.027	0	78.325	1					91.753	1	78.080	-10		
30.5	89.791	0	92.376	-1	78.219	0			89.502	-1	92.104	5	77.984	1		
31.5	90.070	1			78.116	0			89.781	3	92.456	6	77.877	-2		
	90.352	-1			78.014	-5			90.063	6	92.813	8	77.779	0		
	90.637	-4			77.922	-4										
	90.932	0			77.836	0			90.628	0	93.530	6				
	91.229	1			77.749	-1			90.919	0	93.896	6				
	91.529	3			77.669	0			91.217	3	94.263	4				
	91.831	0	94.941	3	77.591	-1			91.518	5	94.639	6				
	92.140	2	95.321	2	77.520	1			91.817	2	95.015	4				
	92.454	5	95.700	-4	77.453	3			92.124	3	95.393	1				
40.5			96.091	-3					92.434	2	95.777	0				
41.5			96.487	0					92.745	-1	96.163	-2	77.070	12		
			96.885	1					93.065	1	96.558	0	77.005	7		
			97.283	-1					93.380	-6	96.959	4	76.947	6		
			97.693	4					93.708	-3	97.356	1	76.891	2		
			98.095	-3							97.763	4	76.843	3		
	94.740	2	98.507	-3					94.374	0	98.164	-2	76.790	-6		
	95.082	1	98.924	-2					94.711	0	98.576	-2				
	95.428	1	99.345	-1					95.050	-3	98.990	-3				
	95.778	0	99.769	-1					95.396	-1	99.409	-3				
50.5	96.132	0	400.197	-1					95.743	-3	99.834	-1				
51.5	96.490	-1							96.096	-2						
	96.856	3							96.454	0						
	97.220	1							96.813	-1						
	97.591	2							97.179	1						
	97.965	2					80.607	-2	97.546	1						
	98.340	-1					80.876	-6	97.918	0						
	98.723	0					80.954	-4	98.295	2						
	99.106	-3					81.034	-4	98.670	-1						
	99.496	-2					81.119	-2	99.053	-1						
60.5	99.888	-3							99.437	-3						
61.5									99.830	-1						
							81.706*	-1								
							81.820*	2								
							81.937*	4								
							82.058*	6								
							82.189*	14								
70.5							82.305*	4								
71.5							82.437*	6								
			410.572	6												
			11.082	1												
			11.596	-2												
			12.115	-4												
			12.638	-7												
80.5																
81.5																
									410.799	1						
									11.284	-1						
									11.775	0						
									12.268	0						
90.5									12.766	0						
91.5									13.268	2						

TABLE IIC—*Continued*

				2-2				
J	R_1	Δν	R_2	Δν	P_1	Δν	P_2	Δν
1.5								
10.5								
			16 386.281	1				
			86.559	-3				
			86.846	-2				
	16 385.805	-2						
	86.028	-1	87.732	1				
	86.257	2	88.032	0				
20.5			88.336	-2				
21.5			88.646	-1				
			88.964	5				
	87.444	2						
	87.692	2						
	87.946	3						
	88.197							
					16 377.746	-3		
					377.636	0		
30.5					377.522	0		
31.5					377.417	-2		
	89.534	0			377.320	2		
	89.817	0			377.220	1		
	90.099	0			377.124	-1		
					377.034	1		
	90.679	2			376.947	0		
	90.980*	9			376.861	-4		
	91.275*	5			376.789	4		
	91.570*	-1			376.713	3		
40.5	91.881*	4			376.639	1		
41.5	92.190*	4			376.574*	3		
	92.504*	5			376.516*	9		
					376.453*	5		
					376.393*	1		
					376.340*	1		
					376.290*	-1		
					376.244*	-3		
					376.201*	-5		
					376.161*	-8		
50.5	95.136*	-2						
51.5	95.486*	1						
	95.832*	-2						
	96.189*	0						
	96.544*	-2						
	96.905*	-2						
	97.272	-1						
	97.637	-4						
	98.009	-5						
	98.388	-2						
60.5	98.770	0						
61.5	99.155	0						
	99.546	5						
	99.936	3						

similar to those for the other calcium halides. The vibrational structure of the transitions, particularly for low v, is very diagonal. The $\Delta v \neq 0$ CaBr Franck–Condon factors are, respectively, larger and smaller than those for CaF (*12*) and CaI (*24*). As for the other calcium halides, the $v \neq 0$ sequences of CaBr become significantly stronger at high v.

Rotation–vibration analysis for two isotopes of CaBr allows a test of the usual isotopic relationships between parameters (*16*). The agreement between our experimental isotopic parameter ratios and those predicted from the reduced masses is satisfactory ($<3\sigma$).

Brown and Watson (*25, 26*) showed that it is possible to separate A_D (effective)

TABLE III

Spectroscopic Constants of CaBr (in cm^{-1})

State	Isotope	v	B_v	$D_v \times 10^8$	A_v	$A_{D_v} \times 10^5$	p_v	$p_{D_v} \times 10^7$	$q_v \times 10^4$	o_v[a]	γ_v	$\gamma_{D_v} \times 10^7$
$B^2\Sigma^+$	$Ca^{79}Br$	2	0.09539098(203)	4.350(38)							-0.069922(62)	2.58[b]
		1	0.09584311(50)	4.451(13)							-0.069544(42)	2.56(22)
		0	0.09629057(71)	4.398(15)							-0.068988(38)	2.58(14)
	$Ca^{81}Br$	2	0.09460563(227)	4.344(44)							-0.069309(62)	2.40[b]
		1	0.09505133(63)	4.364(17)							-0.068738(65)	1.64(29)
		0	0.09549450(84)	4.385(18)							-0.068359(37)	2.40(14)
$A^2\Pi$	$Ca^{79}Br$	1	0.09508517(252)	4.2132(82)	59.067(1)	-3.646(53)	-0.068379(37)	1.799(145)	-1.2766(478)	-5.310		
		0	0.09551790(47)	4.2142(29)	59.139(1)	-3.091(15)	-0.067349(31)	1.552(55)	-1.3189(79)	-5.212		
	$Ca^{81}Br$	1	0.09429751(238)	4.1580(81)	59.065(1)	-3.540(40)	-0.067838(37)	1.957(155)	-1.2061(453)	-5.311		
		0	0.09472437(55)	4.1341(37)	59.136(1)	-3.002(16)	-0.066815(34)	1.580(58)	-1.2826(85)	-5.214		
$X^2\Sigma^+$	$Ca^{79}Br$	2	0.093460329(86)	4.13247(171)							0.00295781(56)	
		1	0.093861918(19)	4.13136(38)							0.00298013(55)	
		0	0.094264488(18)	4.13028(38)							0.00300355(49)	
	$Ca^{81}Br$	2	0.092688896(71)	4.0670[c]							0.0029312[c]	
		1	0.093085456(25)	4.06503(52)							0.00295515(73)	
		0	0.093482984(13)	4.06300(28)							0.00297907(53)	

Numbers in parentheses are 1σ uncertainties.

[a] Calculated from unique perturber relationship $o_v = \frac{A_v p_v}{8B_v}$. (Ref. 4)

[b] Fixed at value for $v = 0$.

[c] Fixed at values linearly extrapolated from $v = 0$ and 1.

TABLE IV

Measured Line Positions of $\Delta v \neq 0$ Bands of $B^2\Sigma^+ - X^2\Sigma^+$ Transition (in cm^{-1})

$Ca^{79}Br$

	0-1	1-2	1-0	2-1
J	P_1	P_1	R_1	R_1
17.5		16 097.423 0		16 668.504 0
		97.281 0		68.720 0
		97.154 9		
20.5		97.001 -1		
21.5		96.882 -2		68.938 1
		96.757 -4		69.159 0
		96.637 -6		69.376 -8
				69.619 7
				69.839 -3
		96.317 -1		70.075 0
	16 094.766 0	96.217 -2		70.304 -8
	94.674 0	96.116 -8		70.551 -1
	94.587 0	96.036 0		70.802 7
30.5	94.504 -1	95.952 1		71.043 2
31.5	94.427 0	95.873 1		
	94.355 0	95.797 -1		
	94.288 0	95.724 -2		
	94.225 1	95.663 2		
	94.167 0	95.603 2	16 677.504 -2	
	94.114 0	95.548 4	77.849 0	
	94.066 1	95.499 5	78.197 0	
	94.023 1	95.448 1	78.543 1	
	93.984 0		78.896 0	
40.5	93.950 0		78.250 -1	
41.5	93.922 1		79.609 1	
			79.970 1	
			80.334 0	
			80.698 -2	
			81.072 1	
52.5	93.928 0			
	93.958 1			
	93.993 1			
	94.032 1			
	94.077 1			
	94.126 1			
	94.180 1			
	94.239 1			79.474 1
60.5	94.302 0			79.808 -1
61.5	94.370 1			80.148 0
	94.443 0			80.491 3
	94.522 -1			80.831 -2
	94.605 -1			80.182 -2
	94.693 -1			
	94.785 -1			

Numbers following each line position are obs.-calc. in units of $10^{-3} cm^{-1}$

$Ca^{81}Br$

	0-1	1-0	2-1
J	P_1	R_1	R_1
39.5	16 095.199 -1	16 677.621 -1	
40.5	95.167 2	77.974 -1	
41.5	95.136 -2	79.688 0	
		79.049 -1	
		79.412 2	
		79.782 0	
		80.154 2	
		80.524 -1	
		80.900 2	
48.5		81.283 2	
57.5			16 677.541 1
			77.867 0
			78.198 2
			78.524 -4
60.5			
61.5			78.864 0
			-
			79.543 -1
			79.888 0
			80.236 1
			80.581 -3
			80.940 3
			81.293 1

TABLE V

Measured CaBr Bandheads (in Å)

	$B^2\Sigma^+ - X^2\Sigma^+$			
	$Ca^{79}Br$		$Ca^{81}Br$	
v'-v"	P_1	P_2	P_1	P_2
0-1	6 211.830	6 210.762	6 211.364	6 210.308
1-2	6 211.297	6 210.204	6 210.832	6 209.748
2-3	6 210.846	6 209.734	6 210.390	6 209.284
3-4	-	6 209.368	-	6 208.910
0-0	6 104.491	6 103.246	6 104.476	6 103.246
1-1	6 104.613	6 103.337	6 104.593	6 103.337
2-2	6 104.820	6 103.510	6 104.800	6 103.510
3-3	6 105.112	6 103.777	6 105.092	6 103.766
4-4	6 105.485	6 104.125	6 105.460	6 104.110
1-0	6 001.133	5 999.585	6 001.530	5 999.996
2-1	6 001.966	6 000.370	6 002.356	6 000.776
3-2	-	6 001.237	-	6 001.635
4-3	-	6 001.823	-	-

	$A^2\Pi - X^2\Sigma^+$					
	$Ca^{79}Br$					
	$^2\Pi_{1/2} - {}^2\Sigma^+$			$^2\Pi_{3/2} - {}^2\Sigma^+$		
v'-v"	P_{1ee}	Q_{12ef}	P_{12ff}	P_{21ee}	Q_{2ef}	P_{2ff}
0-0	6 278.057	6 278.026	6 286.210	6 253.208	6 253.165	6 258.707
1-1	6 277.112	6 277.079	-	6 252.274	6 252.233	-
	$Ca^{81}Br$					
	$^2\Pi_{1/2} - {}^2\Sigma^+$			$^2\Pi_{3/2} - {}^2\Sigma^+$		
	P_{1ee}	Q_{12ef}	P_{12ff}	P_{21ee}	Q_{2ef}	P_{2ff}
0-0	6 278.057	6 278.026	6 286.138	6 253.208	6 253.165	6 258.653
1-1	6 277.112	6 277.079	-	6 252.274	6 252.233	-

The accuracy of heads is 0.004Å

into "true" γ and A_D, provided that isotopic data are available.[4] In our case, the isotopic A_D values differ so slightly that this procedure is unlikely to give reliable values. The values of γ_0 (true) and A_D obtained from isotopic data are:

$$\gamma_0 = 0.057 \text{ cm}^{-1}$$

$$A_{D_0} = 4.1 \times 10^{-5} \text{ cm}^{-1}.$$

The pure precession estimates of γ_0 (true) is (*26*):

$$\gamma_0 = -p/2 = 0.034 \text{ cm}^{-1}.$$

In order to check the significance of some of our small parameters, we have used the customary Pekeris (*18*) and Kratzer relations (*16*). The values are included in the table of equilibrium constants (Table VII) and the agreement is 10% for $\omega_e x_e$ and <1% for D_e.

In addition, the program of Albritton *et al.* (*27*) was used (along with the RKR curve) in order to calculate D_v values. The agreement is excellent (±0.1%) even in the excited states. For example, calculated values for the $v = 0$ levels of $Ca^{79}Br$ are $D_0 = 4.128 \times 10^{-8}$ cm^{-1} ($X^2\Sigma^+$), 4.220×10^{-8} cm^{-1} ($A^2\Pi$), and 4.404×10^{-8} cm^{-1} ($B^2\Sigma^+$). The calculated values were fit to extract D_e and β_e and these values are included in Table VII.

Veseth (*28*) has derived a formula for estimating γ_{D_v}:

$$\gamma_{D_v} = \gamma_v\left[\frac{A_{D_v}}{A_v} - \frac{2D_v}{B_v} - \frac{B_\Pi - B_\Sigma}{\Delta\nu_{\Pi\Sigma}}\right].$$

For γ_{D_0} of $Ca^{79}Br$, this equation gives 2.25×10^{-7} cm^{-1}, which is close to the experimental value, 2.58×10^{-7} cm^{-1}. A similar expression for p_{D_v} gives $p_{D_0} = 2.16 \times 10^{-7}$ cm^{-1}. The unique perturber model requires $p_D \approx \gamma_D$. The γ_D and p_D values predicted by Veseth's equations are in reasonable agreement with each other and fall *between* the respective experimental values. However, our phenomenological A_D is a factor of 7 larger than the value predicted by Merer's relationship (*29*).

[4] This separation of γ and A_D is supposed to yield a γ value which contains both spin–rotation and second-order spin–orbit contributions.

TABLE VI

CaBr Band Origins (in cm^{-1})

	$B^2\Sigma^+-X^2\Sigma^+$		$A^2\Pi-X^2\Sigma^+$	
v'v"	$Ca^{79}Br$	$Ca^{81}Br$	$Ca^{79}Br$	$Ca^{81}Br$
0-1	16 099.066(5)	16 100.237(2)		
1-2	16 100.533(6)			
0-0	16 383.114(1)	16 383.108(1)	15 959.774(1)	15 959.770(1)
1-1	16 382.901(1)	16 382.895(1)	15 962.230(1)	15 962.213(1)
2-2	16 382.462(1)	16 382.464(1)		
1-0	16 666.956(1)	16 665.777(2)		
2-1	16 664.835(5)	16 663.674(2)		

Numbers in parentheses are 1σ uncertainties.

TABLE VII

Equilibrium Constants (in cm^{-1})

	$X^2\Sigma^+$		$A^2\Pi$		$B^2\Sigma^+$	
	$Ca^{79}Br$	$Ca^{81}Br$	$Ca^{79}Br$	$Ca^{81}Br$	$Ca^{79}Br$	$Ca^{81}Br$
T_e	0	0	15 958.41(10)[c,d]	15 958.41(10)[c,d]	16 383.137(6)	16 383.133(8)
ω_e	285.7315(92)	284.5430(135)	288.56(20)[c,d]	287.35(20)[c,d]	285.7465(92)	284.5491(143)
$\omega_e x_e$	0.8400(39)	0.8333(48)	-	-	0.9540(39)	0.9428(50)
$\omega_e x_e$ (Pekeris)	0.9480(2)	0.9315(4)	1.024(9)	1.014(14)	1.046(8)	1.040(4)
B_e	0.094466141(32)	0.093682111(68)	0.0957343(20)	0.0949378(20)	0.0965151(20)	0.0957166(11)
α_e	0.000403551(38)	0.000398496(80)	0.0004327(20)	0.0004269(29)	0.0004483(15)	0.0004437(8)
$\gamma_e \times 10^7$	4.91(38)	4.84(80)	-	-	-	-
$D_e \times 10^8$	4.129737(90)	4.06199(68)	4.2142(29)[b]	4.1341(37)[b]	4.398(15)[b]	4.385(18)[b]
$D_e \times 10^8$ [f] (calc.)	4.1271(1)	-	4.213(3)	-	4.4013(2)	-
$D_e \times 10^8$ (Kratzer)	4.1303(2)	4.0619(4)	4.215(7)	4.145(6)	4.4043(6)	4.3322(4)
$\beta_e \times 10^{11}$	1.084(76)	2.03(80)	-	-	-	-
$\beta_e \times 10^{11}$ [f] (calc.)	1.88(7)	-	14.4(2)	-	5.7(1)	-
γ_e (spin-rotation)	0.00301484(50)	0.00299103(116)	-	-	-0.068767(79)	-0.068115(63)
$\alpha_\gamma \times 10^4$ [a]	-0.2289(31)	-0.2392(126)	-	-	-4.84(55)	-4.64(45)
p_e	-	-	-0.066834(64)	-0.066304(70)	-	-
α_p [a]	-	-	-0.001030(68)	-0.001023(71)	-	-
A_e	-	-	59.175(1)[d]	59.172(1)[d]	-	-
α_A [a]	-	-	-0.072(1)[d]	-0.071(1)[d]	-	-
R_e(Å)	2.593585	2.593584	2.5764	2.5764	2.56769(3)[e]	2.56759(2)[e]

Numbers in parentheses are 1σ uncertainties.

[a] Our α's (except α_e) are defined by $X_v = X_e + \alpha_X(v + \frac{1}{2})$ with X = γ, p, A.

[b] D_0 is listed rather than D_e.

[c] Only 0-0 and 1-1 A-X bands were analyzed so the $\omega_e x_e$ used to obtain T_e and ω_e came from the Pekeris relationship. This relationship seems to work to about 10% accuracy in the other CaBr states. The uncertainties of T_e and ω_e reflect this fact.

[d] The o parameter used in our fit is completely correlated with the band origin and the spin-orbit constant. Thus this parameter affects the values of T_e, ω_e, A_e, and α_A given in this table.

[e] The values for R_e were computed from the B_e values by correcting for q^Σ. The unique perturber model predicts $q^\Sigma = {}^e-q^\Pi$ so $B_e^\Sigma = B_e+q^\Pi$ (4).

[f] Calculated using the program of Ref. 27.

TABLE VIII

Franck–Condon Factors for $Ca^{79}Br$

$B^2\Sigma^+ - X^2\Sigma^+$

v' \ v"	0	1	2	3	4	5
0	0.919	0.075	0.006	-	-	-
1	0.080	0.774	0.129	0.016	0.002	-
2	0.001	0.148	0.652	0.167	0.030	0.004
3	-	0.003	0.207	0.551	0.193	0.040
4	-	-	0.006	0.257	0.466	0.208
5	-	-	-	0.009	0.300	0.395

$A^2\Pi - X^2\Sigma^+$

v' \ v"	0	1	2	3	4	5
0	0.968	0.031	0.001	-	-	-
1	0.032	0.907	0.058	0.003	-	-
2	-	0.062	0.851	0.080	0.006	-
3	-	-	0.089	0.801	0.099	0.009
4	-	-	0.001	0.114	0.756	0.115
5	-	-	-	0.001	0.137	0.715

Only values greater than 0.001 are listed.

V. SUMMARY

The spectrum of CaBr is typical of alkaline earth halides and, more generally, transitions involving nonbonding electrons. Laser excitation spectroscopy with narrow band detection allows the dense and badly overlapped spectrum to be analyzed. Narrow band detection allows the experimenter to select the branches and bands of greatest interest from the jumble of overlapped lines in the spectrum. The use of a continuously tunable single-mode, dye laser provides very high-quality data ($\pm 0.003\text{-cm}^{-1}$ accuracy).

Simultaneous fitting of the $A-X$, $B-X$ and microwave data reduces correlations in the molecular constants. The combined fit molecular constants obey the expected isotopic relations. The molecular constants allow accurate Franck–Condon factors to be calculated. These Franck–Condon factors are required for the conversion of laser-induced fluorescence intensities into molecular populations in monitored chemical reactions. The molecular constants, particularly lambda doubling and spin–rotation parameters, provide some insight into the orbital structure of CaBr. The A and B states form a unique perturber pair with $l_{eff} = 1.24$, suggestive of $3d$ character in these states.

ACKNOWLEDGMENTS

We are greatly indebted to K. Möller and Professor T. Törring for providing us with their microwave data in advance of publication. P. F. Bernath was supported, in part, by a Natural Sciences and Engineering Research Council of Canada postgraduate fellowship. The MIT portion of this research was supported by Grants AFOSR-76-3056, NSF CHE-78-18427, and CHE-78-10178, NATO 1177.

Note added in proof. Uncertainties for the $X^2\Sigma^+$ state constants, γ_v (Table III), γ_e and α_γ (Table VII), must be increased by a factor of 50 because unresolved hyperfine structure in the $N \sim 15$-mm wave data caused a systematic error in measured spin splittings. The effect on all other parameter values and uncertainties is negligible. Higher-precision radiofrequency measurements of $X^2\Sigma^+$ state hfs and γ values by W. J. Childs, D. R. Cok, G. L. Goodman, and L. S. Goodman indicated the existence and source of this problem.

RECEIVED: November 13, 1980

REFERENCES

1. O. H. WALTERS AND S. BARRATT, *Proc. Roy. Soc. Ser. A* **118**, 120–137 (1928).
2. B. ROSEN, *in* "International Tables of Selected Constants," Pergamon, New York, 1970.
3. R. E. HARRINGTON, Ph.D. thesis, Berkeley, 1942.
4. R. N. ZARE, A. L. SCHMELTEKOPF, W. J. HARROPP, AND D. L. ALBRITTON, *J. Mol. Spectrosc.* **46,** 37–66 (1973). The fitting routines used were generated by R. C. Stern and revised by T. H. Bergeman, R. A. Gottscho, and A. J. Kotlar.
5. K. MÖLLER AND T. TÖRRING, private communication.
6. S. GERSTENKORN AND P. LUC, "Atlas du Spectre d'Absorption de la Molecule d'Iode," CNRS, Paris, 1978.
7. S. GERSTENKORN AND P. LUC, *Rev. Phys. Appl.* **14,** 791–794 (1979).
8. J. B. WEST, R. S. BRADFORD, JR., J. D. EVERSOLE, AND C. R. JONES, *Rev. Sci. Instrum.* **46,** 164–168 (1975).
9. M. S. SOREM AND A. L. SCHAWLOW, *Opt. Commun.* **5,** 148–151 (1972).
10. P. F. BERNATH, P. G. CUMMINS, AND R. W. FIELD, *Chem. Phys. Lett.* **70,** 618–620 (1980).
11. P. F. BERNATH, B. PINCHEMEL, AND R. W. FIELD, *J. Chem. Phys.*, in press.
12. M. DULICK, P. F. BERNATH, AND R. W. FIELD, *Canad. J. Phys.* **58,** 703–712 (1980).
13. L. E. BERG, L. KLYNNING, AND H. MARTIN, *Phys. Scr.* **21,** 173–178 (1980).
14. W. DEMTRÖDER, *in* "Case Studies in Atomic Physics" (M. R. C. McDowell and E. W. McDaniels, Eds.), Vol. 6, North-Holland, Amsterdam, 1976.
15. C. LINTON, *J. Mol. Spectrosc.* **69,** 351–364 (1978).
16. G. HERZBERG, "Spectra of Diatomic Molecules," 2nd. ed., p. 107, Van Nostrand, New York, 1950.
17. A. J. KOTLAR, R. W. FIELD, J. I. STEINFELD, AND J. A. COXON, *J. Mol. Spectrosc.* **80,** 86–108 (1980).
18. C. L. PEKERIS, *Phys. Rev.* **45,** 98–103 (1934).
19. R. J. LEROY, private communication.
20. R. N. ZARE, *J. Chem. Phys.* **40,** 1934–1944 (1964).
21. P. F. BERNATH AND R. W. FIELD, *J. Mol. Spectrosc.* **82,** 339–347 (1980).
22. L. E. BERG, L. KLYNNING, AND H. MARTIN, *Phys. Scr.*, in press (1980).
23. R. S. MULLIKEN AND A. CHRISTY, *Phys. Rev.* **38,** 87–119 (1931).
24. D. E. REISNER, P. F. BERNATH, AND R. W. FIELD, *J. Mol. Spectrosc.*, in press.
25. J. M. BROWN AND J. K. G. WATSON, *J. Mol. Spectrosc.* **65,** 65–74 (1977).
26. J. M. BROWN, E. A. COLBOURN, J. K. G. WATSON, AND F. D. WAYNE, *J. Mol. Spectrosc.* **74,** 294–318 (1979).
27. D. L. ALBRITTON, W. J. HARROP, A. L. SCHMELTEKOPF, AND R. N. ZARE, *J. Mol. Spectrosc.* **46,** 25–36 (1973).
28. L. VESETH, *J. Phys. B.* **3,** 1677–1691 (1970).
29. A. J. MERER, *Mol. Phys.* **23,** 309–315 (1972).